Mineralogical Magazine, February 2016, Vol. 80(1), pp. 157–174

Reconstruction of an Ordovician seafloor volcano-hydrothermal system: a case study from the Copper Coast, southeastern Ireland using field, geochemical and fluid inclusion data

C. Breheny[1,*], K. R. Moore[2], A. Costanzo[1] and M. Feely[1]

[1] Earth and Ocean Sciences, School of Natural Sciences, National University of Ireland, Galway, Ireland.
[2] Camborne School of Mines, College of Engineering, Mathematics and Physical Sciences, University of Exeter, Penryn Campus, Treliver Road, Penryn, Cornwall TR10 9EZ, UK.

[*Received 25 February 2014; Accepted 30 March 2015; Associate Editor: Craig Storey*]

ABSTRACT

Volcanic rocks in south County Waterford include flow-top hyaloclastite, pillow lavas and peperite, which are formed typically by sub-aqueous eruption or intrusion into unconsolidated sediment. Element mobility in wet sediment during emplacement of volcanic intrusions was reconstructed on a variety of spatial scales using bulk-rock and mineral analysis. Magma-sediment and magma-water interactions enhanced hydrothermal alteration. The chemistry of chlorite was a function of mixing between an Fe-rich magmatic fluid and a Mg-rich meteoric fluid. Chlorite geothermometry yields temperatures of formation between 230 and 388°C compatible with other metamorphic indicators. Fluid inclusion microthermometric data from genetically-related mineralized quartz veins reveal a hydrothermal vein mineralization event that occurred at lower temperatures during the end stage of volcanic activity. A convection driven mixing trend reflects the trapping of co-existing brine with entrained seawater concomitant with, the late stages of emplacement of the Bunmahon Volcano intrusions.

Keywords: Chlorite geothermometry, peperite, fluid inclusions, hydrothermal alteration, Ireland.

Introduction

The southeast volcanic belt in Ireland (Fig. 1) comprises Ordovician volcanic and sedimentary rocks, (e.g. Wilson, 1966) where sulfide mineralization has been mined famously at Avoca and along the Copper Coast (Wheatley, 1971; McConnell, 1987; Cowman, 2005). The volcanic rocks at Avoca in the east reflect rifting in an intra-arc extensional regime (McConnell, 1991), where sulfide mineralization was coeval with volcanic activity (Wheatley, 1971; McConnell, 1987). The Kuroko-style mineralization at Avoca is considered as evidence that more extensive concealed ore bodies of a similar nature may occur elsewhere in the southeastern volcanic belt (Platt, 1977). Approximately 120 km to the southwest are two submarine volcanic centres that have been reconstructed from regional mapping (Stillman and Sevastopulo, 2005) on the southern coast that could potentially have driven mineralizing systems and are thus a target for commercial exploration. The earlier Bunmahon Volcano and later Kilfarassy Volcano are associated with island arc magmatism (Max *et al.*, 1990). Two localities (Fig. 1) that represent volcanic activity proximal (Bunmahon Formation) and distal (Dunabrattin Formation) to the centre of the Bunmahon Volcano (Boland, 1983; Harper and Parkes, 2000) are investigated in this research to constrain better the relationship between volcanic activity, hydrothermal alteration and base-metal mineralization on the Copper Coast.

The volcanic belt is in the core of a major Caledonian synclorium (Shannon, 1976) and is

* E-mail: breheneee@hotmail.com
DOI: 10.1180/minmag.2015.079.7.09

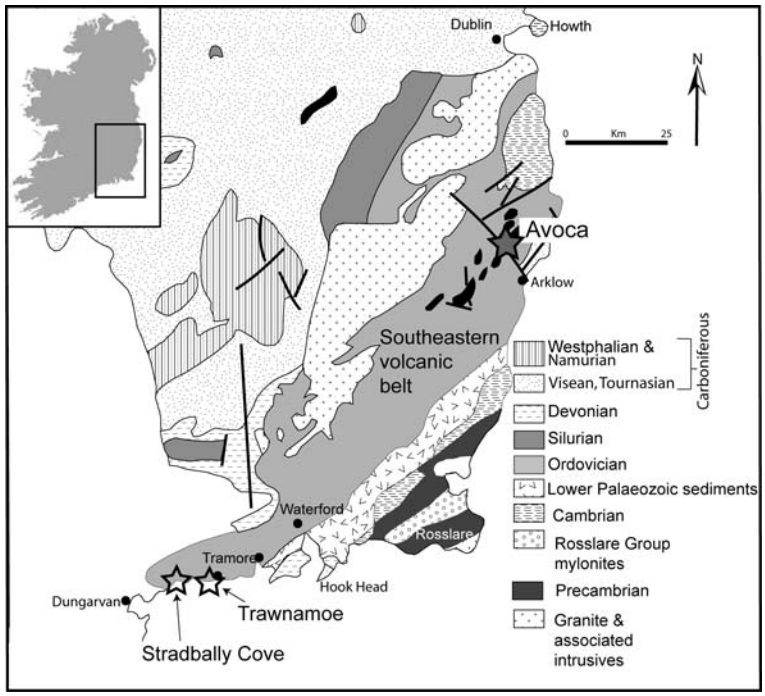

FIG. 1. Maps showing the position of the southeastern volcanic belt and the location of study areas on the Copper Coast: Trawnamoe and Stradbally Cove.

metamorphosed to greenschist- and sub-greenschist-facies assemblages, with a pervasive cleavage developed throughout (Stillman and Williams, 1979). The lithologies are arc-related subaqueous extrusive rocks, shallow-level intrusive rocks and tuffs representing gravity flows of pyroclastic or epiclastic origin (Stillman and Maytham, 1973; Scheiner, 1974; Downes, 1975; Stillman and Williams, 1979; Boland, 1983; Fritz and Stillman, 1996) and rare sub-aerial eruptions (Stillman, 1971). Regional-scale mapping has been concerned largely with the relationship of volcanic activity to the closure of the Iapetus Ocean but has revealed localities that preserve evidence of contemporaneous magmatism and sedimentation (Scheiner, 1974; Stillman *et al.*, 1974; Downes, 1975; Boland, 1983; McConnell *et al.*, 1991; McConnell, 2000). Of particular interest in this study are the lithologies that display evidence of subaqueous volcanism and magma-water and magma-sediment interaction, which will provide evidence of heat energy and fluid mobility in a potential mineralizing system. Mineral alteration assemblages are investigated particularly near the interface between magmatic and sedimentary end members within peperite, in order to isolate ocean-floor alteration from Caledonian metamorphism.

Variation in chlorite composition has been related to distance from VHMS deposits, with higher temperature chlorite close to the deposit being predominantly Mg-rich and the Fe/Mg ratio generally increasing from the deposit centre to the margins (Hendry, 1981; Reed, 1997; Gifkins *et al.*, 2005). Thus chlorite geothermometry has been applied to a variety of rock types to determine formation conditions (Cathelineau and Nieva, 1985; Kranidiotis and MacLean, 1987; Cathelineau, 1988; Jowett, 1991; Zhang *et al.*, 1997). We consider the merits of chlorite geothermometers as applied to rocks of the Bunmahon Volcano and correlate the results with alternative methods of estimating the thermal conditions in the rocks hosting mineral veins. Vein mineralization of the Copper Coast is siliceous with disseminated pyrite, chalcopyrite, sphalerite and galena (Wheatley, 1971). An extensive study of fluid inclusions in sulfide-bearing sheeted mineral veins is used to constrain the source of fluids in the mineralizing system and relate the thermal conditions of lithological alteration to the conditions of mineral vein formation.

https://doi.org/10.1180/minmag.2015.079.7.09 Published online by Cambridge University Press

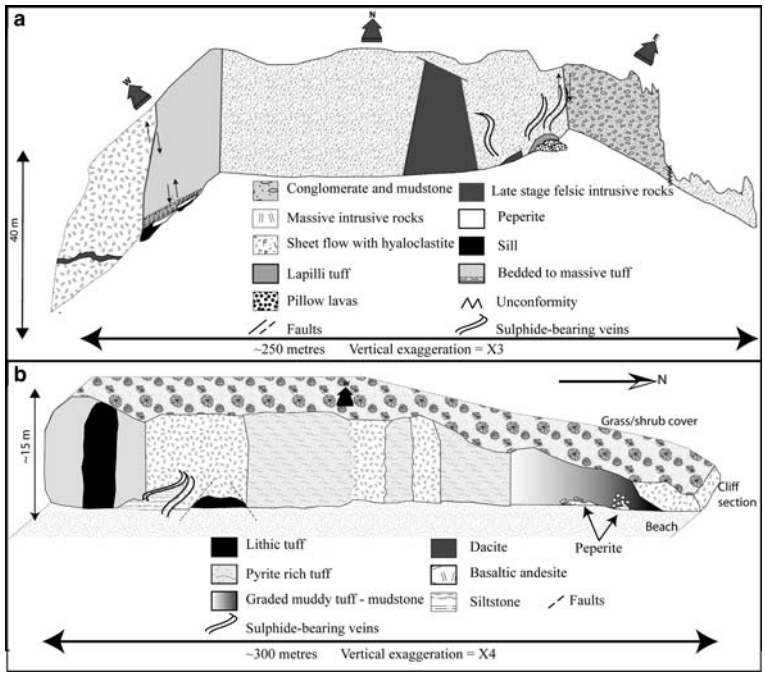

FIG. 2. Geology sketch maps across coastal cliff sections from (*a*) Trawnamoe and (*b*) Stradbally Cove, showing the distribution of the main lithologies.

Field and sample characteristics

Localities (Fig. 1) identified within the Bunmahon, Dunabrattin and Campile (of the Kilfarassy volcano) Formations as type sections (Fig. 2) for volcanic activity proximal to the vent and the outer flanks of the Bunmahon volcano are Trawnamoe (52.1343N, 7.3756W) and Stradbally Cove (52.1231N, 7.4619W), respectively. The majority of volcanic rocks at both locations are pyroxene and feldspar-phyric, mafic to intermediate in appearance, and of both sub-volcanic and extrusive nature. The thickness and abundance of hyaloclastite flow tops to sheet flows on the seafloor (Fig. 3*a*) illustrate that significant magma-seawater interaction occurred. The fine-grained intercalated volcaniclastic and volcano-sedimentary rocks have coarse-grained units that contain clasts of juvenile volcanic material. These are most spectacularly developed in peperite that is observed to have several different morphologies including fluidal, blocky and mixed-morphology (Figs 3*b–d*, respectively), which is a function of the composition and temperature of the intruding magma, and the extent of consolidation of the host sediment (Breheny, 2010). Some clasts within fluidal peperite at Trawnamoe are surrounded by a visible rim (up to 1 cm wide) of fluidized sediment caused by development of a vapour envelope (Breheny, 2010) that illustrates the significance of magma-water interactions within, as well as upon, the seafloor. Sedimentary rocks, such as the siltstone and mudstone at Stradbally Cove (Fig. 2*b*) are very Fe-rich, and disseminated pyrite is a common constituent of both volcanic and sedimentary lithologies. Larger clusters or nodules of pyrite appear to have replaced the coarser grained components of both volcanic and sedimentary lithologies (tuff and silty/sandy layers in mudstone). These nodules have chlorite alteration haloes and adjacent quartz veinlets, indicating that they are probably formed by secondary processes. Following extensive fieldwork and petrographic analysis, 22 lithological samples were chosen for bulk-rock analysis and 18 samples for analysis of mineral chemistry – eight from Trawnamoe and ten from Stradbally Cove. Ten of the samples from both localities were taken from the contacts of peperite clast contacts with the host sediment.

Vein mineralization occurs as sulfide-bearing, irregular and sheeted vein swarms hosted within

https://doi.org/10.1180/minmag.2015.079.7.09 Published online by Cambridge University Press

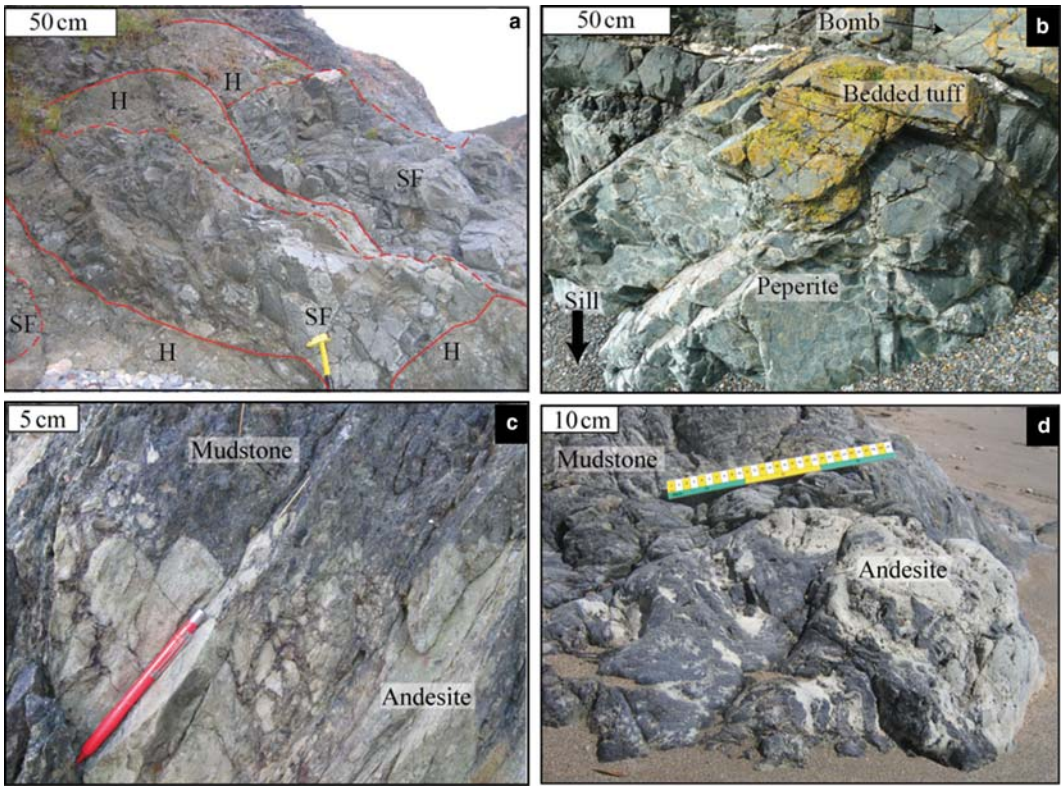

FIG. 3. Field photographs of outcrop displaying magma-sediment interaction observed in Trawnamoe (*a*, *b*) and Stradbally Cove (*c*, *d*). (*a*) Flow-top basaltic andesite sheet flow (SF) with hyaloclastite flow-top (H). (*b*) Fluidal peperite formed in bedded tuff above a basaltic andesite sill. (*c*) Blocky peperite consisting of angular andesite fragments in a honeycomb-textured mudstone. (*d*) Peperite consisting of mixed morphology clasts of andesite within a matrix of muddy tuff.

andesitic sheet flows with hyaloclastic margins in Trawnamoe (Fig. 4*a* and *b*) and in deformed siltstone in Stradbally Cove (Fig. 4*c* and *d*). Six samples from Trawnamoe were used for fluid inclusion studies, where the majority of veins comprising these swarms range in thickness from a few millimetres to 5 cm and have little variation in strike, ranging between 355° and ~25°. The main trend of vein mineralization is vertical to sub-vertical cross-cutting successive sheet flows (Fig. 4*a*). The thicker veins commonly contain angular fragments of country rock (Fig. 4*a*). Individual veins are composed predominantly of quartz or intergrowths of quartz and calcite, with a typical mineral assemblage of quartz + calcite + pyrite ± chalcopyrite ± chlorite. The larger quartz veins tend to exhibit a syntaxial growth pattern with smaller anhedral quartz crystals towards the margin of the vein and larger subhedral crystals within the centre of the vein. Sulfide minerals occur in isolated clusters within the veins (Fig. 4*b*) and are commonly altered to malachite. Three samples were used for fluid inclusion studies from the southern end of Stradbally Cove, where irregular quartz vein swarms are ~40–50 cm wide, and are composed of variable thickness individual veins and minor veinlets. Pyrite is the only sulfide mineral in the samples and it occurs as both a replacement mineral throughout coarser grained units within the siltstone (Fig. 4*c*) and as isolated clusters and stringers along vein margins (Fig. 4*d*). The pyrite nodules in the sedimentary lithologies are best developed in the coarsest beds in the sedimentary succession (Fig. 4*c*), which would have provided the easiest pathways for fluid flow. Individual sub-vertical veins are irregular, with an overall east-west strike. The host siltstone contains convoluted laminations and slumping features

https://doi.org/10.1180/minmag.2015.079.7.09 Published online by Cambridge University Press

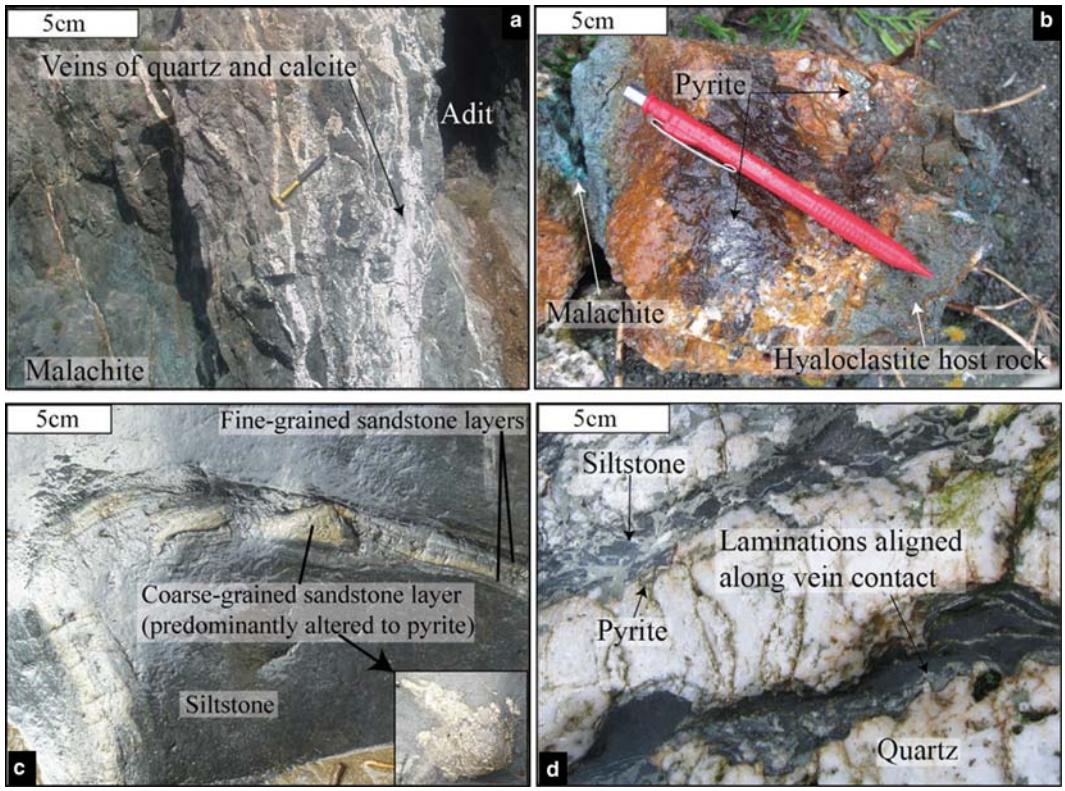

FIG. 4. Field photographs of sulfide mineral occurrences and mineral veins at Trawnamoe (*a*, *b*) and Stradbally Cove (*c*, *d*). (*a*) Sheeted sulfide-bearing vein system hosted by sheet flows. (*b*) Pyrite clusters within sheeted veins on weathered surfaces. (*c*) Pyrite nodules in coarse sandstone layers, interbedded with siltstones and fine sandstones. (*d*) Pyrite-bearing, cross-cutting quartz vein in siltstone, which has laminations aligned parallel to an undulating vein margin. The surface of rocks in (*a*) and (*b*) have secondary malachite formed on exposed rock surfaces.

indicative of soft sediment deformation. Lenses of the host siltstone, with disrupted laminations, have been incorporated into the vein system; some of these laminations are deformed such that they are parallel to the irregular contact with the quartz vein (Fig. 4*d*).

Analytical techniques

Rock samples for bulk-rock geochemistry were prepared in Earth and Ocean Sciences, NUIG, using a multi-acid technique and analysed by inductively coupled plasma mass spectrometry (ICP-MS) at OMAC laboratories in Loughrea, Co. Galway, Ireland. The R^2 test (the square of the Pearson product moment correlation) was applied to determine the errors between published and measured values of four certified reference materials (SY3, SY4, NCS, TILL4); all samples yield values for major, trace and rare-earth elements (*REE*) of 0.93–1, with the majority yielding values of >0.999. Scanning electron microscope (SEM) and electron microprobe analyses (EPMA) were carried out at the Universität de Barcelona, Spain and at the Camborne School of Mines, Cornwall, UK. Preliminary mineral analysis was carried out using a Quanta 200 SEM equipped with Genesis (EDAX) energy dispersive spectroscopy (EDS) and a JEOL JSM-5400LV equipped with an Oxford ISIS EDS system. More detailed microprobe analysis was carried out using a Cameca SX-50 equipped with four wavelength-dispersive spectrometers and automated with *SAMx* software and hardware, using an accelerating voltage of 20 kV and a JEOL JXA-8200 Superprobe, using an accelerating voltage of 15 kV. Microthermometric analysis of fluid inclusions in quartz from

https://doi.org/10.1180/minmag.2015.079.7.09 Published online by Cambridge University Press

TABLE 1. Whole-rock geochemistry of representative samples from Trawnamoe and Stradbally Cove.

	BS6 (massive intrusive)	BS8 (fine-grained dyke)	BS10 (pyrite-rich tuff)	BT2 (peperitic sill)	BT3 (sheet flow with hyaloclastite)	BT7 (peperitic tuff)	BT9 (bedded tuff above peperite)
SiO_2	55.19	47.05	55.37	56.89	55.57	73.75	59.10
Al_2O_3	16.91	15.46	16.92	18.22	17.04	11.44	16.26
CaO	1.88	5.26	0.24	4.70	6.33	0.78	0.36
Cr_2O_3	0.02	0.03	0.05	0.03	0.04	0.00	0.03
Fe_2O_3	6.94	10.18	8.24	9.71	9.04	5.08	11.63
K_2O	0.44	0.54	0.26	0.61	1.29	1.48	2.71
MgO	5.35	9.42	6.03	5.40	7.12	2.92	6.04
MnO	0.09	0.14	0.10	0.16	0.15	0.08	0.18
Na_2O	5.36	1.60	5.36	4.28	3.11	1.91	0.79
P_2O_5	0.15	0.18	0.12	0.11	0.15	0.02	0.02
TiO_2	0.77	1.24	0.75	0.93	0.94	0.11	0.77
LOI	3.31	8.70	4.44	–	–	–	5.00
Total	96.43	99.79	97.88	101.04	100.78	97.57	102.89

S in sample name signifies Stradbally Cove; T in sample name signifies Trawnamoe.

sulfide-bearing and sulfide-absent mineral veins was carried out using a Linkam THMSG 600 heating-freezing stage mounted on an Olympus transmitted light microscope (×10 to ×100 lenses) with a digital camera feeding to a dedicated computer loaded with the *Linksys 32DV* imaging and heating control software. Calibration of the stage was carried out using synthetic FI standards (pure CO_2 and water).

Whole-rock compositions

The compositions of representative magmatic and tuffaceous rocks from Trawnamoe and Stradbally Cove are presented in Table 1 and illustrated in Fig. 5. Regardless of regional greenschist-facies metamorphism, the local evidence for magma-fluid and magma-sediment interaction necessitates that ratios for relatively immobile incompatible elements be used to classify the lithologies (Winchester and Floyd, 1977). The graphs of total alkalis *vs*. silica, silica *vs*. Zr/TiO_2 and Zr/TiO_2 *vs*. Nb/Y illustrate the following: (1) The volcanic rocks form a continuum of compositions from sub-alkaline basalt through to rhyolite, where the more distal intrusions (Stradbally Cove) appear to be more felsic than the proximal intrusions (Trawnamoe). The intrusions on the flank of the volcano (Stradbally Cove) may therefore occur later in the evolution of the volcano above an evolving magma chamber. (2) The intrusive rocks and coeval tuffaceous rocks at Trawnamoe have similar and overlapping compositions, but also illustrate a general fractionation trend supporting the statement above. (3) An enrichment in Si, Na and K is indicated by the more felsic and trachytic nature of the majority of samples within the plot utilizing mobile elements (Fig. 5*c*) as compared to those compositions determined from immobile element ratios (Fig. 5*a*). Silicification is particularly evident in the tuff matrix host to peperite clasts. Silicification of the tuff matrix occurs throughout the peperite lithology and up to 10 cm past the upper contact of peperite clasts with the overlying bedded tuff.

Rare-earth element distribution patterns (Fig. 5*d*) also suggest that limited mobility occurred for certain high-field-strength elements in proximity to intrusions. A significant enrichment in light rare-earth elements (*LREE*) and depletion in heavy rare-earth elements (*HREE*) occurs in the silicified tuff matrix BT7 in fluidal peperite ($La_N/Yb_N = 37.7$). The *LREE* distribution pattern of sample BT7 is similar to the rest of the Bunmahon Formation, while the *HREE* profile is depleted, suggesting that the *HREE* have been removed from the tuff adjacent to intrusions, possibly as a result of peperite-driven fluid migration. The extent of fluidization is indicated by the presence of delicate laminations circumventing the magmatic clasts for up to 1 cm adjacent to clast contacts, indicating that the *REE* mobility is a very local phenomenon related to extreme reorganization of particles in the host tuff. Local-scale element mobility adjacent to peperitic contacts is observed elsewhere

https://doi.org/10.1180/minmag.2015.079.7.09 Published online by Cambridge University Press

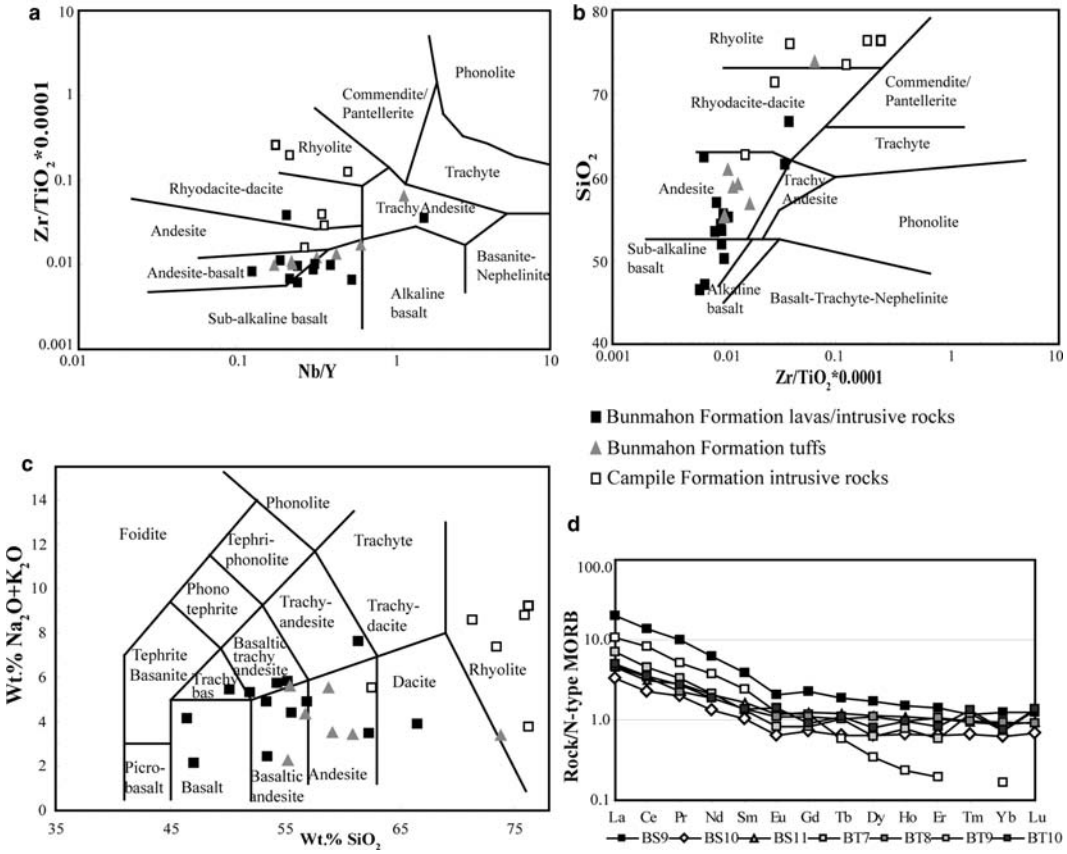

FIG. 5. Whole rock compositions for lithologies of the Bunmahon and Campile Formations (from Trawnamoe and Stradbally Cove) (*a–c*). Bivariate plots (after Winchester and Floyd, 1977 and Le Bas, 1989) displaying continuous variation in compositions from sub-alkaline basalt through to rhyolite. *REE* plot (*d*) showing an anomalous pattern where *REE* have leached from the tuff matrix surrounding peperite in Trawnamoe but remain unaffected in tuff above peperite (sample BT7 = tuff matrix, sample BT9 = bedded tuff above peperite).

on the Waterford coast, where greatest *LREE* enrichment is observed on immediate contact with the rhyolite intrusion and greatest *HREE* ~20 cm away from the intrusion (Diskin and Coetzee, 2010).

Mineral textures and compositions

All volcanic lithologies have been extensively spillitized, resulting in a mineral assemblage of chlorite + epidote + sericite + albite ± pumpellyite ± Fe-oxides. Hydrous alteration minerals high in Fe ± Mg, such as chlorite and epidote, are dominant within peperitic clasts and at the margins of sheet flows and sills, where syn-magmatic interaction with either water or wet sediment might have prevented the crystallization of a primary mineral assemblage dominated by plagioclase and clinopyroxene. Hydrous alteration minerals are also extensively developed within the vitreous components of other volcanic rocks as a result of preferential degradation of glass either associated with syn-emplacement quenching or post-emplacement diagenesis. Late-stage felsic intrusive rocks consist almost entirely of plagioclase, alkali feldspars and quartz, displaying granophyric texture. The dominant plagioclase composition is end-member albite, typical of greenschist-facies metamorphism. The composition of the main mineral phases is presented in Table 2.

Chlorite is ubiquitous throughout all lithologies, occurring as alteration rims around phenocrysts, as inclusions within other secondary minerals

https://doi.org/10.1180/minmag.2015.079.7.09 Published online by Cambridge University Press

(e.g. epidote), as pseudomorphs and as amorphous zones. Amorphous chlorite alteration is particularly well-developed close to magma-sediment contacts due to the higher glass content. The inclusions of chlorite crystals within masses of epidote occur only in peperite (Fig. 6*a*). Chlorite varies in composition from Mg- to Fe-rich (Table 3; Fe/(Fe + Mg) = 0.33–0.63), such that compositions are ripidolite and pycnochlorite according to the classification of Hey (1954). There is a negative relationship between Al^{iv} and Fe number but variations in chlorite composition do not seem to be pre-determined by the host rock type. Alternative reasons for the compositional variation include variable temperatures of alteration (Kranidiotis and MacLean, 1987) or variation in the composition of the hydrothermal fluid (Teagle and Alt, 2004).

Two different chlorite geothermometry techniques were employed (Kranidiotis and MacLean, 1987; Zang and Fyfe, 1995) both of which are variations of the original empirical approach suggested by Cathelineau (1988) and incorporates co-variation in Fe and Al^{iv} content. Each method yields a wide temperature range (230°C–316°C, using the method of Zang and Fyfe, 1995; 262°C–388°C using the method of Kranidiotis and MacLean (1987) (Fig. 7). As these calculations are based on formulae that were devised for active geothermal fields, they may not necessarily yield accurate values for chlorite within Ordovician age rocks and therefore the use of chlorite geothermometers is best used in conjunction with other methods to determine temperatures, such as fluid inclusion studies.

Pumpellyite is developed locally within intrusive rocks, peperite clasts (close to the magma-sediment interface) and bedded tuff, and is commonly associated with other hydrous alteration minerals. Pumpellyite crystals occur as inclusions within epidote phenocrysts (Fig. 6*b*), as alteration rims around chlorite phenocrysts and as elongate and occasionally stubby crystals (up to 100 μm) within the groundmass (Fig. 6*c*).

Epidote occurs within all sills and irregular intrusive rocks with peperitic margins but most extensively within the magmatic clasts of the peperite at Trawnamoe, as small stubby to elongate epidote phenocrysts (Fig. 6*c*). Those that have ragged, altered edges are generally found in association with abundant chlorite alteration and rare pumpellyite (Fig. 6*b*). Epidote abundance decreases rapidly from peperite clast margins to the centre of peperite clasts and within the coherent sill. Glomeroporphyritic masses of epidote are Ca- and Fe-rich and probably (along with

TABLE 2. Compositions of feldspar, albite, chlorite, epidote and pumpellyite minerals in tuff (BT9), sill (BT2, BS6), peperite clasts (BT15a, b, d) and mudstone (BS4).

	Feldspar		Albite		Chlorite					Pumpellyite			Epidote		
Oxide wt.%	Tuff matrix (BT9)	Sill gmas (BT2)	Clast gmas (BS13)	Sill gmas (BT2)	Sill g-mas (BT2)	Sill xta (BS6)	Clast g-mas (BT15b)	Clast xtal (BS13)	Tuff xtal (BT9)	Mudstone matrx (BS4)	Clast xtal (BT15a)	Clast xtal (BT15b)	Clast xtal (BT15d)	Sill xtal (BS6)	Sill xtal (BT2)	Clast xtal (BT15d)
SiO_2	62.85	71.20	72.49	65.3	28.52	29.74	27.18	25.08	27.71	23.26	37.84	38.57	39.27	38.17	38.49	37.58
TiO_2	0.16	0.01	0.11	–	0.05	0.02	0.01	0.09	0.02	0.02	0.08	0.03	0.07	0.04	0.03	0.07
Al_2O_3	23.67	20.31	18.96	28.17	20.51	17.81	21.46	23.54	22.20	23.25	23.87	26.71	26.59	22.59	24.65	23.25
FeO	3.81	0.10	0.13	1.16	25.39	20.20	24.92	27.85	25.56	31.53	13.65	9.99	10.01	14.10	12.75	13.13
MnO	0.01	0.01	0.01	0.04	0.41	0.34	0.55	0.38	0.47	0.32	0.54	0.11	0.30	0.12	0.57	0.15
MgO	1.74	–	0.05	0.37	16.36	22.99	15.54	12.56	11.92	11.53	0.38	–	–	0.01	0.05	–
CaO	0.05	0.07	0.42	0.45	0.05	0.09	0.06	0.06	0.04	0.01	22.62	23.65	23.51	23.78	23.27	23.91
Na_2O	0.07	8.02	7.29	3.84	0.05	0.01	0.02	0.04	0.02	0.04	–	–	–	0.01	0.01	–
K_2O	6.93	0.03	0.43	3.33	0.01	0.05	0.02	0.02	0.46	0.01	0.01	0.03	0.01	0.01	–	0.02
Total	99.34	99.82	99.93	102.7	91.37	91.29	89.86	89.69	88.41	90.01	99.02	99.10	99.79	98.84	99.84	98.12

https://doi.org/10.1180/minmag.2015.079.7.09 Published online by Cambridge University Press

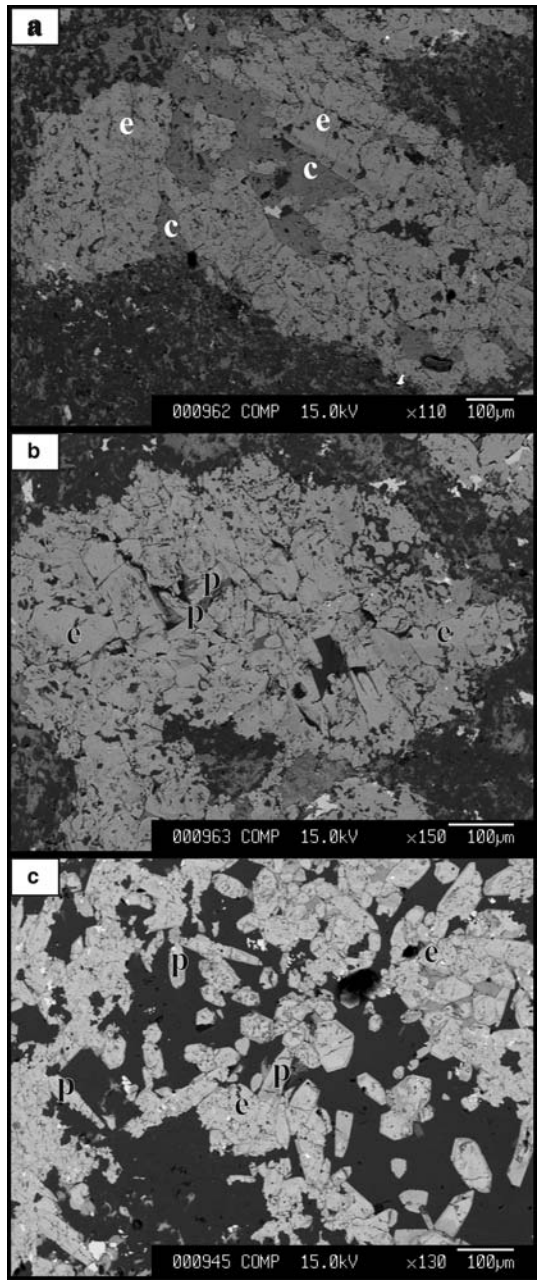

FIG. 6. Back-scattered electron images of the alteration mineral assemblage and textures in spillitized mafic rocks. (*a*) Chlorite inclusions in epidote masses within a clast of fluidal peperite (sample BT15). (*b*) Fine-grained peperitic clast containing pumpellyite inclusions within epidote crystals (sample BT15). (*c*) Masses of epidote and stubby pumpellyite crystals hosted within a microcrystalline feldspar-rich groundmass of a mafic sill (BT2). Note the competent sill contains larger, euhedral crystals (*c*) that are significantly less altered than those found in peperite clasts (*a* and *b*), due to a combination of quenching and later degradation of glass. c = chlorite; e = epidote; p = pumpellyite.

https://doi.org/10.1180/minmag.2015.079.7.09 Published online by Cambridge University Press

TABLE 3. Representative compositions of chlorite from each lithology analysed and number of ions calculated on the basis of 28 oxygens and a tetrahedral occupancy of eight.

Sample	BS28	BT15	BS13	BT9	BT10	BS6	BS4
SiO_2	24.68	25.34	25.77	26.26	27.76	29.50	23.26
TiO_2	0.07	0.04	0.05	0.05	0.10	0.04	0.02
Al_2O_3	24.85	21.61	24.02	21.66	20.59	20.30	23.26
FeO	26.51	24.93	25.22	28.17	25.79	21.63	31.53
MnO	0.28	0.53	0.31	0.45	0.48	0.32	0.32
MgO	11.83	14.43	13.14	11.80	17.68	21.12	11.53
CaO	0.09	0.10	0.03	0.06	0.09	0.05	0.01
Na_2O	0.03	0.03	–	–	0.04	0.01	0.04
K_2O	0.01	0.02	0.01	0.01	0.01	0.01	0.01
Total	88.35	87.03	88.55	88.45	92.58	92.06	90.02
Number of ions on the basis of 28 oxygens							
Si	5.17	5.38	5.34	5.55	5.53	5.70	4.95
Ti	0.01	0.01	0.01	0.01	0.01	0.01	–
Al^{iv}	2.83	2.62	2.66	2.45	2.47	2.30	3.05
Al^{vi}	3.31	2.78	3.21	2.94	2.36	2.33	2.78
Fe	4.65	4.42	4.37	4.98	4.30	3.50	5.61
Mn	0.05	0.10	0.05	0.08	0.08	0.05	0.06
Mg	3.70	4.56	4.06	3.72	5.25	6.09	3.66
Ca	0.02	0.02	0.01	0.01	0.02	0.01	–
Na	0.01	0.01	–	–	0.02	–	0.02
K	–	0.01	–	–	–	–	–
$Fe^{\#}$	0.56	0.49	0.52	0.57	0.45	0.36	0.61

$^{\#}$Fe = Fe/(Fe + Mg) where Fe is total iron expressed as Fe^{2+}.
BS28 = sill; BT15 = peperite clasts; BS13 = peperite clasts; BT9 = bedded tuff; BT10 = peperitic sill; BS6 = competent intrusive rock; BS4 = mudstone.

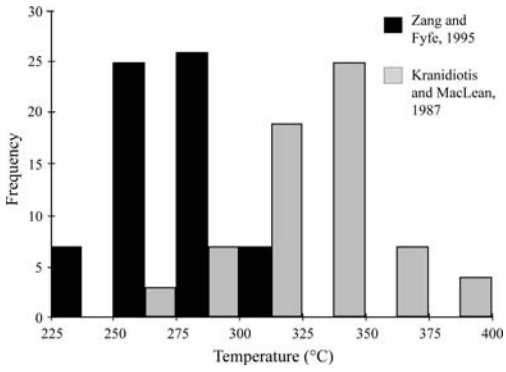

FIG. 7. Frequency histogram showing the variation in temperature estimates from chlorite geothermometry using the method of Zang and Fyfe (1995) where $T = 106.2 \times Al^{iv}$ corrected + 17.5, where Al^{iv} corrected = $Al^{iv} - (0.88 \times [Fe/(Fe + Mg)] - 0.34)$ and Kranidiotis and MacLean (1987) where $T = 106\ Al^{iv}$ corrected + 18, where Al^{iv} corrected = $Al^{iv} + (0.7 \times [Fe/(Fe + Mg)])$.

Fe-Mg chlorite) represent secondary replacement of original clinopyroxene. Occasional crystals of epidote are incorporated into the host tuff matrix of peperite, probably representing incorporation of minor mafic glass fragments during peperite formation.

Fluid inclusion studies

Fluid inclusions were studied in the sulfide-bearing sheeted vein mineralization. Four fluid inclusion (FI) types were identified in quartz, based on paragenetic classification and the physical state of major phases present at room temperature. Type 1 are two-phase liquid-rich inclusions, with a degree of fill between 0.75 and 0.95, recognized as primary due to large size (~6–20 μm) and isolation (Fig. 8*a*,*b*,*d*) within the host crystal (Roedder, 1984). Type 2 are also two-phase liquid-rich FIs but they are smaller than the primary inclusions (2–9 μm). They occur as trails within annealed

https://doi.org/10.1180/minmag.2015.079.7.09 Published online by Cambridge University Press

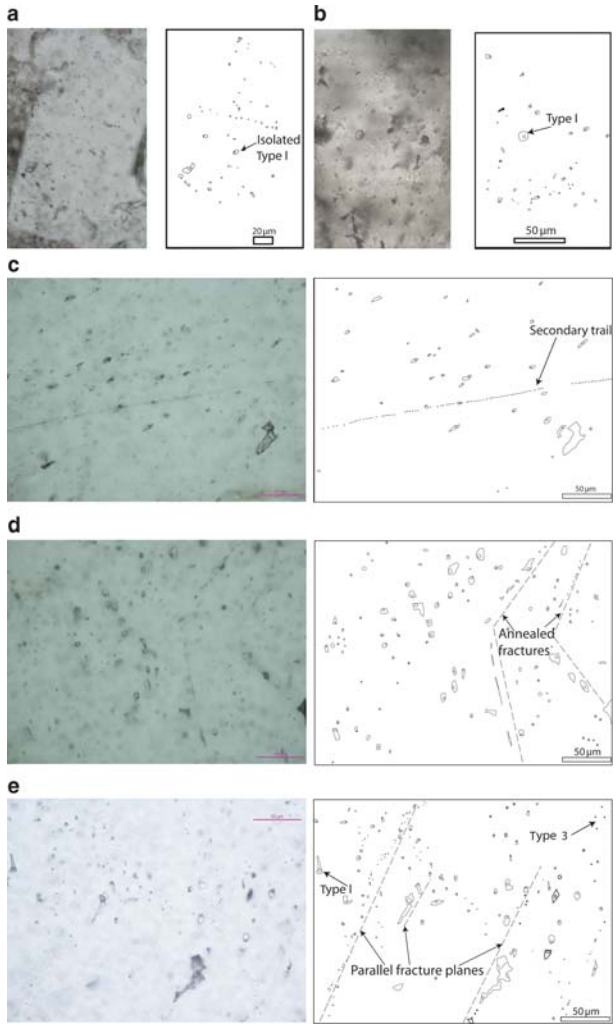

FIG. 8. Photomicrographs of quartz-hosted fluid inclusions from sulfide-bearing vein mineralization at Trawnamoe (*a*, *b*) and Stradbally Cove (*c*, *d* and *e*). Isolated, large, primary Type 1 fluid inclusion (*a*–*d*) and smaller, secondary Type 2 fluid inclusions are two-phase. Type 2 and monophase Type 3 are aligned along annealed fractures (*c*, *d*).

fractures and are classified as secondary (Fig. 8*c*). Type 3 are monophase liquid inclusions (Fig. 8*e*). These are rare and occur within some of the same trails as Type 2 (Fig. 8*c*) and are also classified as secondary. Type 4 are two-phase liquid-rich pseudosecondary inclusions occurring in trails that do not cut crystal boundaries (Fig. 8*d*).

Microthermometry has been carried out on a total of 240 primary Type 1 inclusions from the sulfide-bearing sheeted quartz veins from Trawnamoe (n = 168) and Stradbally Cove (n = 72). Fluid inclusions from Trawnamoe yield T_H values that range from 104.4°C to 219.4°C, with an average of 147.4°C (Fig. 9*a*). Salinities (determined from a total of 25 inclusions) range from 4.8 to 19.05 eq. wt.% NaCl with an average of 13.5 eq. wt.% NaCl (Fig. 9*b*). Fluid compositions calculated for FIs from Trawnamoe correspond to either H_2O–NaCl–KCl or H_2O–$MgCl_2$ as determined from the temperatures of first ice melting (T_{FM} = –24.6°C to –35°C).

Fluid inclusions from Stradbally Cove yield T_H that range from 103°C to 243.9°C, with an average of 170.6°C (Fig. 9*a*). Salinities (determined from 33 inclusions) range from 3.7 to 13.7 eq. wt.%

https://doi.org/10.1180/minmag.2015.079.7.09 Published online by Cambridge University Press

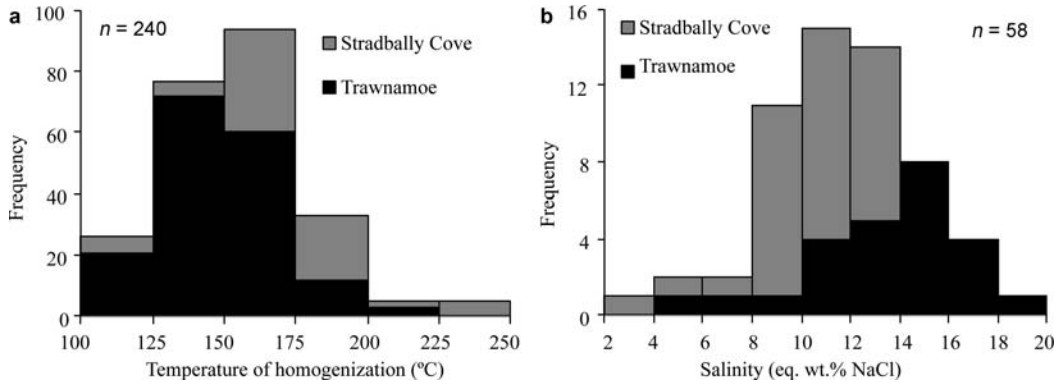

FIG. 9. Frequency distribution histograms showing (*a*) the temperature of homogenization (T_H) and (*b*) salinity of Type 1 fluid inclusions at Trawnamoe and Stradbally Cove.

NaCl with an average of 10.4 eq. wt.% NaCl (Fig. 9*b*). Fluid inclusion compositions calculated from Stradbally Cove range between H_2O–NaCl–$NaSO_4$, H_2O–NaCl–KCl and H_2O–$MgCl_2$ (T_{FM} = –22.5°C to –31°C).

The majority of the T_H values for both localities range between 125 and 175°C (Fig. 9*a*). The majority of salinity values range between 8 and 16 eq. wt.% NaCl (Fig. 9*b*). A bivariate plot of Type 1 T_H-Salinity pairs (Fig. 10) displays a mixing trend between a high *T* (~200°C), low salinity (~10 eq. wt.% NaCl) fluid and a relatively low *T* and high salinity (~20 eq. wt.% NaCl) fluid. These data was used to construct isochores to assist in the investigation of PT conditions of Type 1 fluid trapping. Isochores were constructed using the programmes *BULK* and *ISOC* (Bakker, 2003) using T_H and salinity values for the two end-member fluids (fluid 1:T_H ~200°C and salinity ~10 eq. wt.% NaCl; fluid 2: T_H ~150°C and salinity ~20 eq. wt.% NaCl) estimated from the T_H-Salinity bivariate plot in Fig. 10. Independent temperature estimates from the chlorite thermometry (~230–388°C, this study) and the regional metamorphic temperature range appropriate for prehnite-pumpellyite to lower greenschist facies (300–450°C; Best, 2006) are included with the isochores in Fig. 11. Intersections between the isochores and the independent thermometric estimates yield fluid trapping pressures >2 kb for both fluids (Fig. 11). These pressures are incompatible with a sub-seafloor hydrothermal system. However, the T_H values for fluid 1 range up to 250°C and overlap the lower end of the range typical for this type of hydrothermal system. Steele-MacInnis *et al*., (2012) state that quartz-hosted fluid

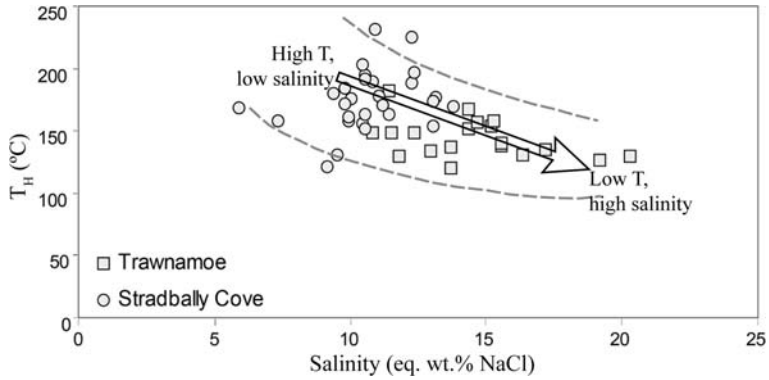

FIG. 10. Salinity *vs*. T_H bivariate plot for Type 1 FI showing a mixing trend between a high temperature, low salinity fluid and a lower temperature, high salinity fluid.

https://doi.org/10.1180/minmag.2015.079.7.09 Published online by Cambridge University Press

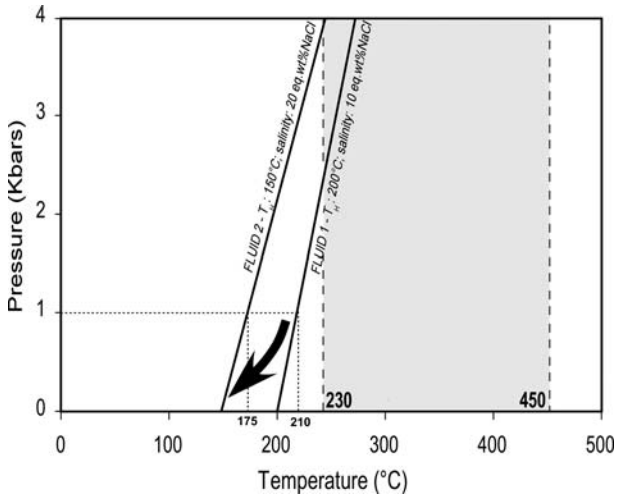

FIG. 11. Pressure - temperature space showing Type FI isochores for the two fluids. The temperature range for chlorite formation and prehnite–pumpellyite facies is also shown for comparison.

inclusions trapped near sub-seafloor hydrothermal vents are liquid rich with T_H values of 200–400°C and salinities typical of seawater ~3.2 eq. wt.% NaCl. Similar fluid inclusion microthermometric data are also recorded from volcanogenic massive sulfide deposits (Steele-MacInnis *et al*., 2012) and active hydrothermal mounds (Tivey *et al*., 1998). Depth of fluid trapping is shallow and significantly less than 1 kb. e.g. <500 m. Therefore, there is an apparent disconnect between the microthermometric data for the Type 1 FI and the independent geothermometers i.e. chlorite thermometer – isochore intersections indicate that the veins formed at pressures >2 kb and are not related to a sub-seafloor hydrothermal system. However, unequivocal field relationships show that the veins represent a shallow emplacement event at a late stage in the system, prior to felsite emplacement.

Discussion

The primary mineral assemblage of the host volcanic and sedimentary sequence has been altered to chlorite, albite, sericite and epidote, with minor calcite, which is characteristic of spillitization (Cann, 1969) while the formation of secondary pyrite in both sedimentary and volcanic rocks is indicative of propylitization, where late-stage alteration is caused by fluids derived from either later intrusive bodies or vein-forming fluids (Coats, 1940). Therefore, the range and combination of alteration minerals could be potentially indicative of either early-stage metasomatism or late-stage hydrothermal alteration or metamorphism. Variables that can be used to isolate magmatism-related alteration and regional metamorphism include time, temperature and the composition of associated fluids.

Relative timing of vein mineralization and alteration

Sulfide-bearing sheeted vein systems are found within both volcanic (hyaloclastite) and sedimentary (siltstone) hosts. Highly angular fragments of the host volcanic rocks at Trawnamoe indicate some degree of lithification had taken place prior to vein formation. The vertical to sub-vertical nature of the sheeted veins are similar to feeder zone veins, where fracturing of the host rock is due to overpressure of the mineralizing fluid (Zierenberg *et al*., 1998). The sulfide-bearing veins are perpendicular to the stratigraphy and cross-cut the early volcanic succession, whereas nearby faulted contacts of late-stage felsic intrusive rocks, with locally developed cataclastite, remain essentially unmineralized. These faulted contacts represent weaknesses that were not utilized by the mineralizing fluids and therefore sulfide vein mineralization occurred prior to emplacement of felsic rocks, probably at the later stages of the volcanic system as a result of a prolonged elevated geothermal gradient. Deformation of siltstone lenses incorporated into

https://doi.org/10.1180/minmag.2015.079.7.09 Published online by Cambridge University Press

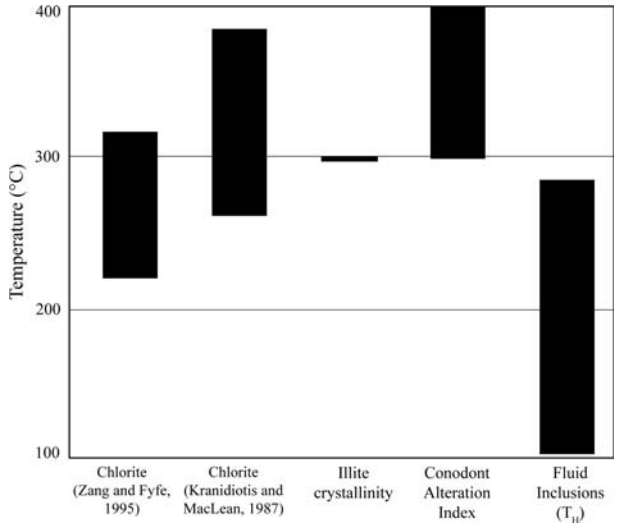

FIG. 12. Comparisons of temperature determinations for alteration and hydrothermal activity in volcanic rocks along the south coast of Waterford. Chlorite = temperatures determined from chlorite geothermometry (this study); Illite crystallinity = temperatures determined from illite crystallinity in Ordovician volcanic rocks from the southeastern volcanic belt (Diskin, 1997); Conodont Alteration Index = temperatures determined from the conodont alteration index in sedimentary rocks along the southeast coast (Bergstrom, 1980); T_H = temperatures determined from fluid inclusions (this study).

the sulfide-bearing veins at Stradbally Cove occurred as a result of disaggregation of the lithified host rock. Disaggregation indicates that the host siltstone and fine sandstone was broken along individual grain boundaries and that the degree of cementation was probably 'patchy', which is commonly the case during the early stages of lithification (Parnell and Kelly, 2003). Therefore, vein formation again followed consolidation of the sediments, probably in an early epigenetic environment, similar to the sheeted vein systems at Trawnamoe. Extensive field studies and analysis of rock textures (Breheny, 2010) has shown that the intrusions at Stradbally Cove were emplaced throughout the lithification history of the sedimentary host rocks, such that an early epigenetic classification of vein mineralization would suggest it could have overlapped temporally with peperite formation (syn-volcanic vein mineralization). Structurally controlled planar veins from both localities are not associated with alteration and are probably of a later stage than the sulfide-bearing sheeted vein systems. The syn-volcanic interpretation of mineralization suggests that an elevated geothermal gradient throughout the Bunmahon Volcano and its environs was enhanced by renewed volcanic activity at the Kilfarrasy Volcano, resulting in the generation and regional circulation of a hydrothermal fluid.

Temperature of alteration and vein mineralization

The composition of chlorite varies significantly between lithologies, with substitution occurring between Si and tetrahedral Al (Al^{iv}) and between Mg and Fe, and with a negative relationship between Al_{iv} and Fe number. This co-variation, and the absence of a relationship between Fe number and host lithology, suggests that geothermometers taking Mg, Fe and Al^{iv} content into account is most reliable. Additional methods can be used to validate the choice of chlorite geothermometer (Fig. 12). The conodont alteration index (temperature-induced colour change associated with low-grade metamorphism in conodonts) represents a regional heating of 300°C to 400°C within the Ordovician age Tramore Limestone (Bergström, 1980), the base of which is temporally equivalent to the upper parts of the Bunmahon and Dunabrattin Formations. These temperatures are coincident with the chlorite geothermometry results. Illite crystallinity has been used to calculate

https://doi.org/10.1180/minmag.2015.079.7.09 Published online by Cambridge University Press

a narrow range of temperatures at ~300°C (Diskin, 1997) for the regional metamorphism that occurred after the emplacement of the intrusions and that did not overprint the associated enhanced crystallinity at the edges of the aureole (Diskin and Coetzee, 2010). This suggests that the higher calculated chlorite temperature for crystals in glass and peperite clasts, where magma is interacting with water at the time of formation, might provide an estimate of the temperature of fluid associated with emplacement. The mineral assemblage indicates that the volcanic rocks represent a transitional assemblage between prehnite/pumpellyite and sub-greenschist facies, which corresponds to temperatures in the region of 300–450°C (Best, 2006) and correlates well with calculated chlorite temperatures. However, the microthermometric data indicate that the late-stage sulfide-bearing veins may not be temporally related to the chloritization. Isochore intersections with the chlorite thermometer yield pressures incompatible with a shallow volcanic hydrothermal setting for vein emplacement and mineralization. The mixing trend in Fig. 10 results from a hydrothermal vein mineralization event that occurred, at lower temperatures, probably during the end stage of volcanic activity. The higher temperature (~200°C), lower salinity (~10 eq. wt.% NaCl) fluid became more saline (~20 eq. wt.% NaCl) with a concomitant decrease in temperature (~150°C) suggesting the trapping of a coexisting brine with entrained seawater similar to that described by Steele-MacInnis *et al*., (2012).

Element mobility

As stated above, the absence of a relationship between Fe number and host lithology suggests that the composition of the hydrothermal fluid is probably a dominant influence. The Fe/(Fe + Mg) ratio of chlorite (0.33–0.63) is interpreted to reflect the relative proportions of hydrothermal fluid (Fe-rich) and seawater (Mg-rich) present in the system (Lécuyer *et al*., 1995; Reed, 1997; Teagle and Alt, 2004). Figure 13 illustrates the distribution of chlorite compositions with varying Fe number: Fe-rich chlorite is located preferentially close to magmatic clasts in peperite while Mg-Fe chlorites are located preferentially throughout the sedimentary host rocks further from intrusions. Seawater always loses Mg and SO_4^{2-} to the rock in seawater-rock interactions at 300°C, regardless of rock type (Chiba, 1995), which explains the association of Mg-Fe chlorites with pyrite replacement in the Fe-rich host rocks at Stradbally Cove.

The greater abundance of chlorite than epidote indicates a water:rock ratio of ~30 (Reed, 1983). If the volcanic intrusions are syn-sedimentary to early epigenetic, then the intrusions would have driven extensive fluid migration through a poorly consolidated sediment. Pyrite replacement within the coarser-grained units provides evidence for the wide extent of fluid percolation, while the *REE* data suggests that magmatism-driven fluid migration of high-field-strength elements was a local phenomenon. This is entirely consistent with

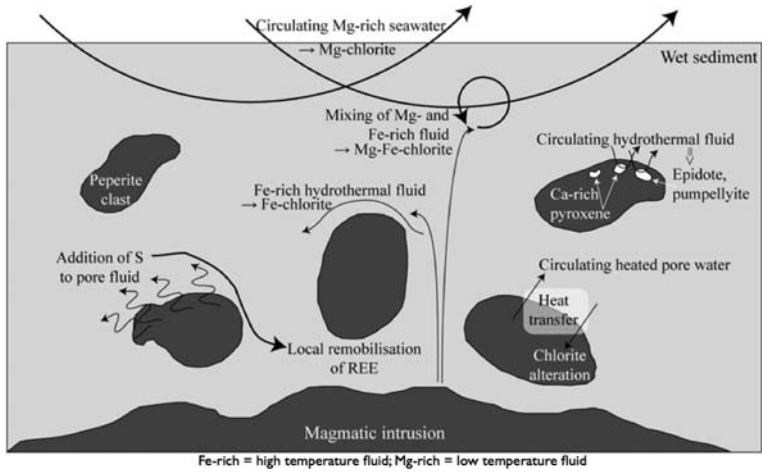

FIG. 13. A schematic illustrating fluid and element migration through wet sediment in the environs of the Bunmahon Volcano, predominantly as a result of peperite formation. Fluids with higher Fe:Mg ratio are of a higher temperature, with decreasing temperature a function of addition of Mg-rich seawater to the hydrothermal fluid.

https://doi.org/10.1180/minmag.2015.079.7.09 Published online by Cambridge University Press

published bulk-rock analysis of sedimentary host rocks with distance from a rhyolite intrusion (Diskin and Coetzee, 2010), which suggests that *REE* mobility occurred during early diagenesis as a function of a fluid passing through unlithified sediment. However, no direct mechanism has been suggested for the preferential mobility of specific *REE* species in this environment. Experiments have shown that aqueous REE complexes at $T < 150°C$ have increasing stability with increasing atomic number, i.e. from La to Lu and with the harder ligands OH^- and CO_3^{2-} (Pearson, 1963; Luo and Byrne, 2001). However, *REE* complexes with the borderline ligand Cl^- decrease in stability with increasing *REE* hardness, i.e. from La to Lu, and increasing temperatures alter the relative hardness of ligands and the relative stability of *REE* species (Luo and Byrne, 2001; Williams-Jones *et al.*, 2012). The implication is that *HREE* complexes with the OH^- ligand flux outwards with migrating fluid, rather than complexes with the Cl^- ligand, at reasonably low temperatures. Thus it appears that the fluid responsible for *REE* remobilization was derived from the unconsolidated sediment rather than from the magmatic intrusion and was mobilized by the heat of intrusion. The short distance of *REE* transport suggests that thermal energy was dissipated rapidly next to individual intrusions but that, on the larger scale, intrusion may have provided the impetus for a more extensive fluid system with large inferred water:rock ratios as suggested previously.

Conclusions

Multiple lines of evidence including field observations, petrographic and geochemical observations, geothermometry and fluid inclusion studies have been used to reconstruct a volcano-hydrothermal mechanism of fluid migration and element mobility. The microscale features associated with peperite rocks and fluid inclusion studies of mineral veins have proven particularly revealing and show that a complex set of interactions between magma, magmatic fluids, wet sediment, seawater and brine contributed to the shallow circulation of fluids in the Ordovician ocean floor.

A model for syn-emplacement fluid migration at the Bunmahon Volcano has been reconstructed as follows. Extensive magma-sediment and magma-water interactions formed pillow lavas, hyaloclastite and peperite. The secondary mineral assemblage varied as a function of whole-rock composition (basalt/sub-alkaline basalt to rhyolite), water/rock ratio and the composition of the fluid. The range of chlorite composition in particular was predominantly controlled by the varying composition of the hydrothermal fluid (Fig. 13): Mg abundance (relative to Fe) increases with increasing seawater component and therefore decreasing temperature. The fluid inclusion data reveals a hydrothermal vein mineralization event that occurred at lower temperatures during the end stage of volcanic activity. A convection driven mixing trend (Fig. 10) probably reflects the trapping of a coexisting brine and entrained seawater concomitant with the late stages of emplacement of the Bunmahon Volcano intrusions.

Acknowledgements

C. Breheny acknowledges the support of a NUIG College of Science Postgraduate Fellowship (2006–2009). The authors thank A. Sherlock and H. O'Donnell for technical support at NUIG, and Xavier Llovet and Gavyn Rollinson at the Universität de Barcelona and Camborne School of Mines, Exeter, respectively for analytical expertise and assistance. They also thank Aurum Exploration for field sampling assistance for fluid inclusion studies and Copper Coast Geopark Geologists Sophie Preteseille and Tina Keating for sampling permission and field access. The authors wish to thank the two anonymous referees for providing comments that helped to significantly improve the manuscript.

References

Bakker, R.J. (2003) Package fluids 1. Computer programs for analysis of fluid inclusion data and for modelling bulk fluid properties. *Chemical Geology*, **194**, 3–23.

Bergström, S.M. (1980) Conodonts as paleotemperature tools in Ordovician rocks of the Caledonides and adjacent areas in Scandinavia and the British Isles. *Geologiska Foereningan i Stockholm. Foerhandlingar*, **102**, 377–392.

Best, M.G. (2006) *Igneous and Metamorphic Petrology.* Blackwell publishing.

Boland, M.A. (1983) *The geology of the Ballyvoyle-Kilmacthomas-Kilfarassy area, County Waterford, with an account of the lower Palaeozoic geology of County Waterford.* PhD thesis, University of Dublin, Trinity College, Dublin.

Breheny, C. (2010) *Volcanic activity, magma-sediment-water interation, hydrothermal alteration and vein mineralisation in south County Waterford.* PhD Thesis, Earth and Ocean Sciences National University of Ireland, Ireland.

https://doi.org/10.1180/minmag.2015.079.7.09 Published online by Cambridge University Press

Bucher, K. and Frey, M. (2002) *Petrogenesis of Metamorphic Rocks.* Springer, New York.

Cann, J.R. (1969) Spillites from the Carlsberg ridge, Indian ocean. *Journal of Petrology*, **10**, 1–19.

Cathelineau, M. (1988) Cation site occupancy in chlorites and illites as a function of temperature. *Clay Minerals*, **23**, 471–785.

Cathelineau, M. and Nieva, D. (1985) A chlorite solid solution geothermometer: The Los Azufres (Mexico) geothermal system. *Contributions to Mineralogy and Petrology*, **91**, 235–244.

Cathles, L.M. (1977) An analysis of the cooling of intrusives by ground-water convection which includes boiling. *Economic Geology*, **72**, 804–826.

Chiba, H. (1995). Chemical modeling of seawater-rock interaction: Effect of rock-type on the fluid chemistry and mineral assemblage. Pp. 469–486 in: *Biogeochemical processes and ocean fluxes in the western pacific* (H. Sakai and Y. Nozaki, editors). Terra Scientific Publishing Company, Tokyo.

Coats, R.R. (1940) Propylitization and related types of alteration on the Comstock Lode [Nevada]. *Economic Geology*, **35**, 1–16.

Cowman, D. (2005) A history of Tankardstown mine, 1850 – c.1875. *Journal of the Mining Heritage Trust of Ireland*, **5**, 3–10.

Diskin, S.M.V. (1997) *Low grade metamorphim of the upper Ordovician rocks of southeast Waterford from Tramore to Stradbally.* MSc thesis, University of Dublin, Trinity College, Dublin.

Diskin, S.M.V. and Coetzee, S.H. (2010) Observations on the effect of proximity to rhyolitic intrusions on kübler index. *Mineraliogia*, **41**, 75–94.

Downes, K. (1975) *The geology of the Ordovician volcanics of County Waterford and southwest County Wexford, Ireland*. PhD thesis, University of Dublin, Trinity College, Dublin.

Fritz, W.J. and Stillman, C.J. (1996) A subaqueous welded tuff from the Ordovician of County Waterford, Ireland. *Journal of Volcanology and Geothermal Research*, **70**, 91–106.

Gifkins, C., Herrmann, W. and Large, R. (2005) *Altered Volcanic Rocks: A Guide to Description and Interpretation.* Centre for Ore Deposit Research, University of Tasmania, Australia.

Harper, D.A.T. and Parkes, M.A. (2000) Ireland. Pp. 52–64 in: *A Revised Correlation of Ordovician Rocks in the British Isles* (F.J. Gregory, editor). Special Report, **24**. Geological Society of London, London.

Hendry, D.A.F. (1981) Chlorites, phengites, and siderites from the Prince Lyell ore deposit, Tasmania, and the origin of the deposit. *Economic Geology*, **76**, 285–303.

Jowett, E.C. (1991) Fitting iron and magnesium into the hydrothermal chlorite geothermometer. *Proceedings of the Geological Association of Canada/Mineralogical Association of Canada/Society of Economic Geology Joint Annual Meeting, Toronto*. Abstract 16, p. A62.

Kranidiotis, P. and MacLean, W.H. (1987) Systematics of chlorite alteration at the Phelps Dodge massive sulfide deposit, Matagami, Quebec. *Economic Geology*, **82**, 1898–1911.

Le Bas, M.J., Le Maitre, R.W., Streckeisen, A. and Zanettin, B. (1989) A chemical classification of volcanic rocks on the total alkali-silica diagram. *Journal of Petrology*, **27**, 745–750.

Lécuyer, C., Grandjean, P. and Martineau, F. (1995) Seawater-sediment-basalt interactions: Stable isotope (H, O) and elemental fluxes within the Ordovician volcano-sedimentary sequence of Erquy (Brittany, France). *Contributions to Mineralogy and Petrology*, **120**, 249–264.

Luo, Y-R. and Byrne, R.H. (2001) Yttrium and rare earth element complexation by chloride ions at 25°C. *Journal of Solution Chemistry*, **30**, 837–845.

Max, M.D., Barber, A.J. and Martinez, J. (1990) Terrane assemblage of the Leinster Massif, SE Ireland, during the Lower Palaeozoic. *Journal of the Geological Society of London*, **147**, 1035–1050.

McConnell, B. (1987) *Geochemistry of Ordovician peralkaline volcanics at Avoca, Co. Wicklow and their regional association*. PhD thesis, University of Dublin, Dublin.

McConnell, B. (2000) The Ordovician arc and marginal basin of Leinster. *Irish Journal of Earth Sciences*, **18**, 41–49.

McConnell, B.J., Stillman, C.J. and Hertogen, J. (1991) An Ordovician basalt to peralkaline rhyolite fractionation series from Avoca, Ireland. *Journal of the Geological Society of London*, **148**, 711–718.

Parnell, J. and Kelly, J. (2003) Remobilization of sand from consolidated sandstones: Evidence from mixed bitumen-sand intrusions. Pp. 505–514 in: *Subsurface Sediment Mobilization.* (P. Van Rensbergen, R.R. Hillis, A.J. Maltman and C.K. Morley, editors). Special Publication **216**. The Geological Society, London.

Pearson, R.G. (1963) Hard and soft acids and bases. *Journal of the American Chemical Society*, **85**, 3533–3539.

Platt, J.W. (1977) Volcanogenic mineralization at Avoca, Co. Wicklow, Ireland, and its regional implications. *The Institute of Mining and Metallurgy and the Geological Society*, **7**, 163–170.

Reed, M.H. (1997) Hydrothermal alteration and its relationship to ore fluid composition. Pp. 303–366 in: *Geochemistry of Hydrothermal Ore Deposits* (H.L. Barnes, editor). John Wiley & Sons.

Roedder, E. (1984) *Fluid Inclusions.* Reviews in Mineralogy, **12**. Mineralogical Society of America, Washington, DC.

https://doi.org/10.1180/minmag.2015.079.7.09 Published online by Cambridge University Press

Scheiner, E.J. (1974) Syndepositional small-scale intrusions in Ordovician pyroclastics, Co. Waterford, Ireland. *Journal of the Geological Society of London*, **130**, 157–161.

Shannon, P.M. (1976) *The petrology and structural relations of some Lower Palaeozoic rocks in southeast Leinster*. PhD thesis, National University of Ireland, Ireland.

Steele-MacInnis, M., Han, L., Lowell, R.P., Rimstidt, J.D. and Bodnar, R.J. (2012) Quartz precipitation and fluid inclusion characteristics in sub-seafloor hydrothermal systems associated with volcanogenic massive sulfide deposits. *Central European Journal of Geosciences*, **4**, 275–286.

Stillman, C.J. (1971) Ordovician ash-fall tuffs from County Waterford. *Scientific proceedings of the Royal Dublin A*, **4** (7), 89–101.

Stillman, C.J. and Maytham, D.K. (1973) The Ordovician volcanic rocks of Arklow head, Co. *Wicklow. Proceedings of the Royal Irish Academy. Section B: Biological, Geological, and Chemical Science*, **73**, 61–77.

Stillman, C.J. and Sevastopulo, G. (2005) *Classic Geology in Europe 6: Leinster.* Terra Publishing, Harpenden, UK.

Stillman, C.J. and Williams, C.T. (1979) Geochemistry and tectonic setting of some upper Ordovician volcanic rocks in east and southeast Ireland. *Earth and Planetary Science Letters*, **41**, 288–310.

Stillman, C.J., Downes, K. and Scheiner, E.J. (1974) Caradocian volcanic activity in east and southeast Ireland. *Scientific Proceeding of the Royal Dublin Soviety*, **6A**, 87–98.

Teagle, D.A.H. and Alt, A.C. (2004) Hydrothermal alteration of basalts beneath the Bent Hill massive sulfide deposit, Middle Valley, Juan de Fuca Ridge. *Economic Geology*, **99**, 561–584.

Tivey, M.K., Mills, R.A. and Teagle, D.A.H., (1998) Temperature and salinity of fluid inclusions in anhydrite as indicators of seawater entrainment and heating in the TAG active mound. Pp. 179–190 in: *Proceedings of the Ocean Drilling Program, Scientific Results* (P.M. Herzig, S.E. Humphris, D.J. Miller and R.A. Zierenberg, editors). Leg 158. College Station, TX (Ocean Drilling Program), doi:10.2973/odp.proc.sr.158.211.1998

Wheatley, C.J. (1971) *Economic geology of the Avoca mineralised belt, SE Ireland and Parys Mountain.* PhD thesis, University of London, London.

Williams-Jones, A.E., Migdisov, A.A. and Samson, I.M. (2012) Hydrothermal mobilisation of the Rare Earth Elements - a tale of "Ceria" and "Yttria". *Elements*, **8**, 355–360.

Wilson, J.T. (1966) Did the Atlantic close and then re-open? *Nature*, **211**, 676–681.

Winchester, J.A. and Floyd, P.A. (1977) Geochemical discrimination of different magma series and their differentiation products using immobile elements. *Chemical Geology*, **20**, 325–343.

Zang, W. and Fyfe, W.S. (1995) Chloritization of the hydrothermally altered bedrock at the Igarapé Bahia gold deposit, Carajás, Brazil. *Mineralium Deposita*, **30**, 30–38.

Zhang, Y., Muchez, P. and Hein, U.F. (1997) Chlorite geothermometry and the temperature conditions at the Variscan thrust front in eastern Belgium. *Geologie en Mijnbouw*, **76**, 267–270.

Zierenberg, R.A., Fouquet, Y., Miller, D.J., Bahr, J.M., Baker, P.A., Bjerkgård, T., Brunner, C.A., Duckworth, R.C., Gable, R., Gieskes, J., Goodfellow, W.D., Gröschel-Becker, H.M., Guèrin, G., Ishibashi, J., Iturrino, G., James, R.H., Lackschewitz, K.S., Marquez, L.L., Nehlig, P., Peter, J.M., Rigsby, C.A., Schultheiss, P., Shanks, W.C., Simoneit, B.R.T., Summit, M., Teagle, D.A.H., Urbat, M. and Zuffa, G.G. (1998) The deep structure of a sea-floor hydrothermal deposit. *Nature*, **392**, (6675), 485–488.

https://doi.org/10.1180/minmag.2015.079.7.09 Published online by Cambridge University Press